Matter

Article

Programmable microwave-driven actuation systems with angle sensitivity and multimodal response

Graphical abstract

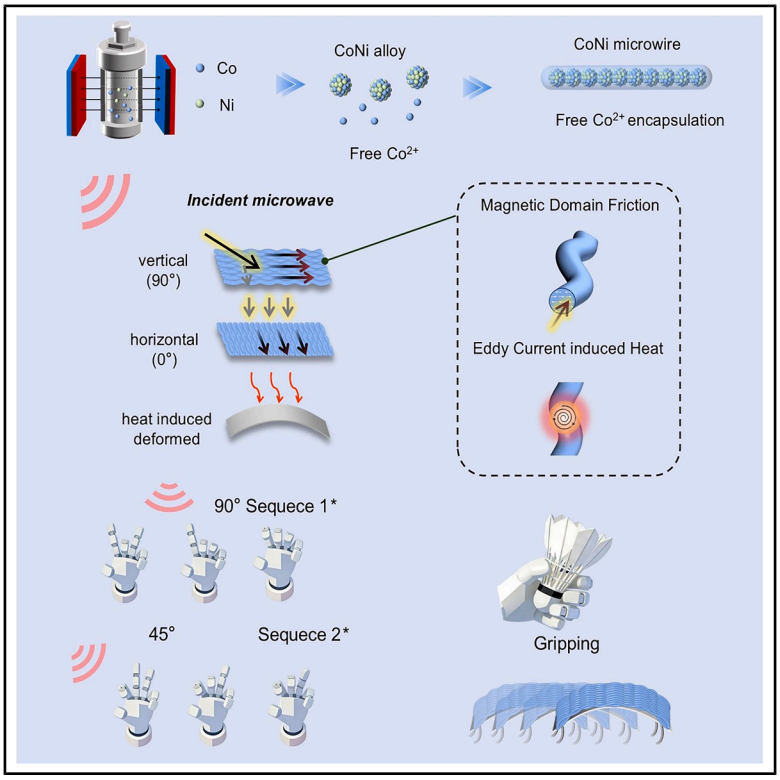

Highlights

- Angle-sensitive CoNi fabrics turn microwaves into local heat
- Material encoding enables programmable MDOF actuation systems
- A single microwave stimulus triggers sequential robotic actions
- Untethered robots achieve adaptive grasping and stable walking

Authors

Meichen Wen, Jizhai Cui, Yandong Wang, ..., Jian Wang, Wenbin You, Renchao Che

Correspondence

wbyou@fudan.edu.cn (W.Y.), rcche@fudan.edu.cn (R.C.)

In brief

Controlling miniature wireless robots often requires bulky equipment or complex signals. This study introduces a novel solution using smart, angle-sensitive metallic fabrics that selectively absorb microwaves based on their orientation. By pairing these fabrics with shape-changing alloys, researchers created programmable robots that walk or grasp objects sequentially under a single, uniform microwave field. This material-driven approach eliminates the need for internal wiring, paving the way for versatile, untethered robots in complex environments.

Development
Practical, real world, technological considerations and constraints

Wen et al., 2026, Matter 9, 103033
December 2, 2026 © 2026 Elsevier Inc. All rights are reserved, including those for text and data mining, AI training, and similar technologies.
https://doi.org/10.1016/j.matt.2026.103033

CellPress

Please cite this article in press as: Wen et al., Programmable microwave-driven actuation systems with angle sensitivity and multimodal response, Matter (2026), https://doi.org/10.1016/j.matt.2026.103033

Matter

CellPress

Article

Programmable microwave-driven actuation systems with angle sensitivity and multimodal response

Meichen Wen,[1,2] Jizhai Cui,[3] Yandong Wang,[1] Chang Zhang,[1] Xiaowei Lv,[1] Xuhui Xiong,[1] Jiazhuan Qin,[1] Zhikai Yan,[1] Gangjie Lian,[4] Jian Wang,[1] Wenbin You,[1,5,*] and Renchao Che[1,*]

[1]Laboratory of Advanced Materials, Shanghai Key Lab of Molecular Catalysis and Innovative Materials, State Key Laboratory of Coatings for Advanced Equipment, College of Smart Materials and Future Energy, Fudan University, Shanghai 200438, China

[2]Materials Genome Institute, Shanghai University, Shanghai 200444, China

[3]International Institute for Intelligent Nanorobots and Nanosystems &State Key Laboratory of Surface Physics, College of Intelligent Robotics and Advanced Manufacturing, Fudan University, Shanghai 200438, China

[4]International Institute for Materials Innovation, Nanchang University, Nanchang 330031, China

[5]Lead contact

*Correspondence: wbyou@fudan.edu.cn (W.Y.), rcche@fudan.edu.cn (R.C.)

https://doi.org/10.1016/j.matt.2026.103033

PROGRESS AND POTENTIAL Smart small-scale actuators hold immense potential for extreme-condition and biomedical operations, yet achieving untethered, programmable, and multi-degree-of-freedom (MDOF) actuation remains a formidable challenge. Conventional wireless strategies, such as magnetic or photothermal actuation, are often constrained by the need for bulky external hardware, shallow penetration depths, or limitations to simple unimodal responses. While microwave actuation offers deep penetration and volumetric heating, selectively controlling MDOF robotic systems typically requires complex external polarization modulation, which hinders practical deployment.

This work introduces a paradigm-shifting material-structure integration strategy to overcome these bottlenecks. By synthesizing highly anisotropic CoNi microwires with an ultrahigh aspect ratio and weaving them into macroscopic fabrics, we created a composite material that exhibits pronounced angle-sensitive microwave absorption. When integrated with shape memory alloys (SMAs), these fabrics translate uniform microwave irradiation into localized, region-specific thermal profiles based purely on their spatial orientation. This material-encoded programmability enables sequential actuation and diverse functional responses under a single, fixed microwave stimulus.

The progress demonstrated here—validated through adaptive grasping manipulators and untethered walking robots—establishes a technically feasible route for antenna-free, passive MDOF actuation. Ultimately, this angle-sensitive design framework unlocks the unique potential of microwave wireless control, paving the way for next-generation autonomous small-scale robots capable of navigating and operating within confined, unstructured, or extreme environments.

SUMMARY

Smart small-scale actuators represent a transformative field with promising applications under extreme and enclosed conditions. Despite great advances, wireless, programmable, and multimodal actuation remains a key challenge. Here, we report a microwave-driven actuation strategy that integrates anisotropic CoNi fabric with shape memory alloys (SMAs) to achieve programmable, multimodal deformation under a single stimulus. The CoNi fabric efficiently converts microwave energy into localized heat through magnetic domain friction and eddy currents, enabling precise, real-time SMA actuation. Owing to its angle-sensitive interaction with microwaves, the system achieves reconfigurable, region-specific heating, thus allowing diverse actuation modes including sequential actuation, object grasping, and terrestrial locomotion. Functional demonstrations using robotic prototypes validate the material's stability and demonstrate its high versatility and strong adaptability to multiple scenarios. This work provides a new design strategy for antenna-free, passive, multi-degree-of-freedom actuation systems and offers a technically feasible route for adaptive operation of such systems in confined, unstructured environments.

All rights are reserved, including those for text and data mining, AI training, and similar technologies.

Please cite this article in press as: Wen et al., Programmable microwave-driven actuation systems with angle sensitivity and multimodal response, Matter (2026), https://doi.org/10.1016/j.matt.2026.103033

INTRODUCTION

The accelerating convergence of flexible electronics[1–4] and advanced smart materials[5–8] has profoundly reshaped the landscape of small-scale actuator and robot,[9–11] unlocking new frontiers in industrial automation, environmental monitoring, and operation within extreme or unstructured environments.[12] Benefiting from their intrinsic compliance, adaptability, and biocompatibility, small-scale robots are increasingly recognized as transformative alternatives to conventional rigid mechanical systems.[13] Nevertheless, the realization of wireless[14] and programmable actuation[15,16] capable of enabling precise and versatile motion control remains a formidable challenge, continuing to limit the broader deployment and functional diversity of such robotic platforms.

Traditional wireless actuation strategies, such as photothermal,[17–19] magnetic,[20–22] electrical,[23,24] and pneumatic[25] approaches have driven significant advances in small-scale robotics, yet each modality remains intrinsically constrained. Photothermal actuation, for example, enables rapid response but is restricted by shallow penetration depth, making it unsuitable for opaque or enclosed environments.[26] Magnetically driven actuation strategies enable relatively long-distance remote control.[27] However, it is dependent on bulky external field-generation hardware and often implies multi-degree-of-freedom (MDOF) manipulation with limited precision.[28,29] Similarly, electrical and pneumatic actuation rely on external wiring or air sources, which hinders miniaturization and reduces adaptability in confined or complex environments. Most of these systems are also restricted to unimodal responses, such as bending or contraction, which limits their versatility for complex robotic tasks. In sharp contrast to the current situation, emerging applications, biomedical intervention,[30] environmental monitoring,[31] and extreme-condition[32] operation, increasingly demand versatile and reconfigurable platforms combined with programmable control.[33] Current solutions integrating multiple stimuli and diverse actuation mechanisms often fall short in providing intrinsic reconfigurability or coordinated, sequential responses,[34–36] while simultaneously introducing greater systemic complexity and reliance on auxiliary peripherals. This limitation highlights the urgent need for a new design paradigm in small-scale robotics that unifies wireless simplicity, programmable control, and functional versatility, ultimately enabling adaptive operation across diverse and unstructured environments.

Microwave actuation has recently emerged as a compelling paradigm owing to its non-contact nature, strong penetration capability, and ability to induce volumetric heating.[37,38] Zhao et al.[39] pioneered a 2.47 GHz far-field microwave-driven parallel robot capable of circular and triangular path motion at 0.4 m under 700 W power, thus breaking through the long-standing control bottleneck of microwave-driven robotic systems. Their approach realized programmable MDOF actuation by tuning the microwave polarization direction to regulate the response of individual bending actuators. However, this method relies on external polarization modulation and conflicts with the design goal of unimodal microwave-driven systems. Consequently, a critical unaddressed challenge remains: achieving diverse and controllable actuation responses under fixed microwave irradiation through rational material selection and structural design.

To address this challenge, we introduce a material-structure integration strategy by combining anisotropic microwave-absorbing fabric with shape memory alloys (SMA). As depicted in the Figure 1A, CoNi microwires are fabricated into highly oriented fabric then coated with SMA, yielding a composite with tunable microwave absorption. Upon microwave irradiation, magnetic domain friction and eddy currents within CoNi microwires convert microwave energy into heat, thereby enabling wireless control of SMA actuation. Figure 1B shows that the anisotropic weaving and stacking of the fabrics produce differentiated heating profiles, which trigger phase transitions in the SMA to achieve controlled bending and deformation. Comparative tests with single-layer and double-layer designs further highlight the role of orientation and architecture in tuning thermal conversion efficiency and response time, thereby enabling multimodal responses. Based on this, promising application scenarios of small-scale robots, including an adaptive grasping manipulator and a stable walking robot, were demonstrated the versatility and multi-scenario adaptability of CoNi fabric (Figure 1C). Our work provides a new design framework for antenna-free and MDOF robots and lays an experimental and theoretical foundation for their application in extreme environment exploration.

RESULTS AND DISCUSSION

Highly aligned, high aspect ratio CoNi microwire

The angle sensitivity microwire under microwave field was fabricated with following steps. First, CoNi microwires were synthesized via a solvothermal method assisted by an external magnetic field with a magnetic flux density of approximately 0.05 T in reactor, which directed the alignment of microwires during growth. The principle of generating ultrahigh-aspect-ratio microwires under magnetic field induction is illustrated in Figure 2A. In this process, a precursor solution with excess cobalt is introduced to initiate the reaction. At the early stage, CoNi alloy nanoparticles are preferentially formed, and under the alignment effect of the external magnetic field, these nanoparticles assemble into CoNi chains. At the initial stage of the reaction, CoNi alloy nanoparticles preferentially nucleate due to the simultaneous reduction of cobalt and nickel ions. Under the guidance of the external magnetic field, these nanoparticles experience magnetic dipole-dipole interactions, which drive their assembly into one-dimensional CoNi chain structures aligned along the field direction. As the reaction proceeds, the concentration of nickel ions decreases, while cobalt ions, which possess higher magneto-crystalline anisotropy and stronger reduction tendency, preferentially deposit at the concave regions and defect sites of the preformed CoNi chains. This stepwise deposition results in the progressive encapsulation of the chains by cobalt, ultimately producing continuous ultralong CoNi microwire with exceptionally high aspect ratios and smooth surfaces. During the proceeds, the bidentate ligand in ethylenediamine, containing two amino groups ($-NH_2$), coordinated with cobalt ions, while the strong magnetocrystalline anisotropy of cobalt further promoted anisotropic crystal growth. The synergistic effect of these factors led to the formation of well-defined nanowires; among them, magnetic-field induction played a predominant role in

Please cite this article in press as: Wen et al., Programmable microwave-driven actuation systems with angle sensitivity and multimodal response, Matter (2026), https://doi.org/10.1016/j.matt.2026.103033

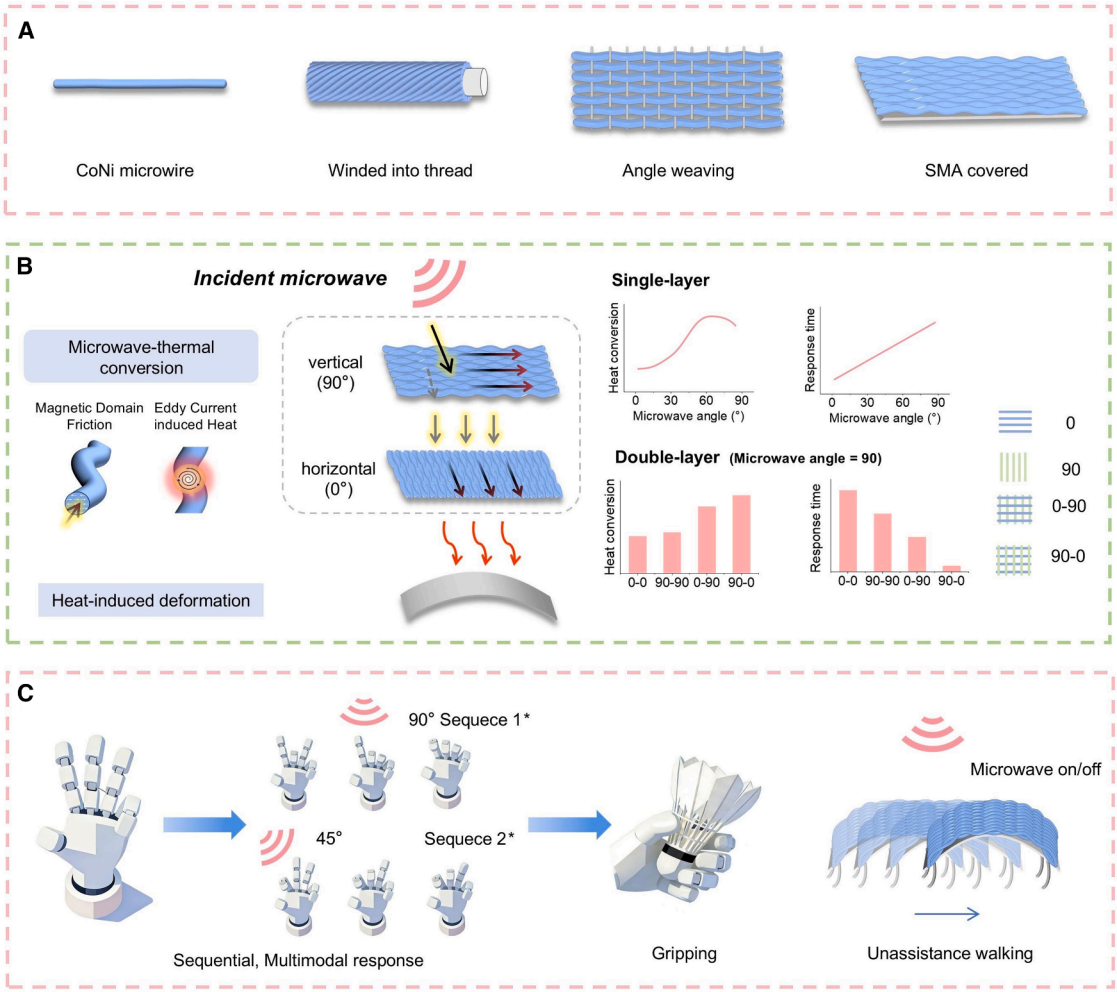

Figure 1. Design and functional mechanism of the CoNi-based small-scale robot

(A) Schematic representation of the manufacturing process for the micro-robot prototype: CoNi microwires are first wound into threads, woven in an oriented manner, and finally coated with a shape memory alloy for enhanced actuation capability.

(B) Operational principle of the CoNi fabric under microwave stimulation. Incident microwaves induce magnetic domain friction and eddy current heating, resulting in directional heat generation. Graphs depict the relationship between microwave angle, heat conversion efficiency, and response time for both single-layer and double-layer arrangements.

(C) Potential applications of the micro-robot, including a controllable robotic hand, ability to gripping item, and walking robot.

directing the one-dimensional morphology. The smooth surface enhances anisotropy localization and facilitates subsequent mechanical processing, such as twisting and weaving, by reducing frictional resistance and preserving structural integrity. These advantages ensure the successful fabrication of CoNi fabrics and establish a solid foundation for their angle-sensitive microwave-responsive behavior.

Subsequently, the obtained CoNi microwires were reduced in a H_2/Ar atmosphere to enhance its crystallinity. As shown in Figures 2B, S1, and S2A, the samples display highly aligned morphology, smooth surfaces, and an average diameter of ~2 μm, yielding an ultrahigh aspect ratio approaching 10,000:1. Energy-dispersive X-ray spectroscopy (EDS) mapping in Figures 2C, S2B, and S2C shows a homogeneous Co/Ni distribution with a thin Co-rich surface layer attributed to slight segregation during reduction, proves the reaction mechanism. Figure 2D combines transmission electron microscopy (TEM) and focused ion beam (FIB) analyses to confirm CoNi alloys surfaces and interiors; high-resolution TEM reveals lattice spacings of 2.03 Å and 1.24 Å corresponding to the fcc (111) and (220) planes of CoNi alloy.[40] The resulting CoNi microwires exhibit centimeter-scale length in Figure 2E, achieving an ultrahigh aspect ratio of over 10,000:1. X-ray diffraction (XRD, Figure 2F) and X-ray photoelectron spectroscopy (XPS, Figures 2G, 2H, and S3) examined the subtle differences in crystal structure and morphology during the morphological evolution process proved a highly crystalline CoNi alloy after reduction.[41] VSM results in Figure 2I demonstrate that the resulting CoNi microwires have a high saturation magnetization of 170.0 emu/g, which confirms the high magnetic properties of the ultrahigh-aspect-ratio

Please cite this article in press as: Wen et al., Programmable microwave-driven actuation systems with angle sensitivity and multimodal response, Matter (2026), https://doi.org/10.1016/j.matt.2026.103033

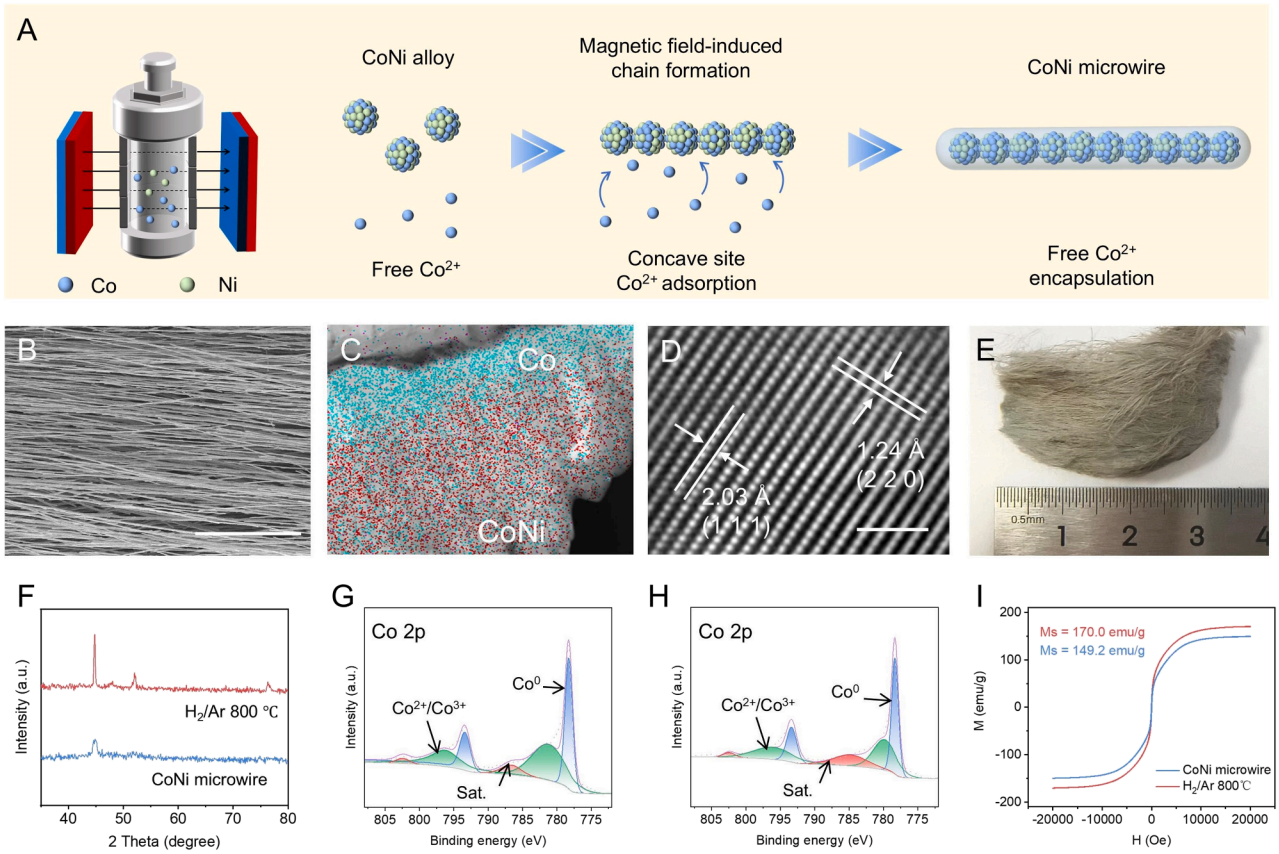

Figure 2. Preparation and characterization of CoNi microwires

(A) Synthesis mechanism of ultra-high aspect ratio CoNi microwires.
(B) SEM images for CoNi microwire, scale bar, 500 μm.
(C) EDX images of CoNi microwires.
(D) HRTEM image of CoNi alloy, scale bar, 1 nm.
(E) Optical photograph of CoNi microwire.
(F) XRD patterns of CoNi microwire before and after reduction.
(G and H) XPS analysis of CoNi microwire (G) before and (H) after reduction.
(I) Room temperature hysteresis loops of CoNi microwire before and after reduction.

microwires. In the preliminary exploration, CoNi was found to be the optimal material for obtaining smooth, well-aligned, and ultrahigh aspect-ratio fibers. Nevertheless, other cobalt-based alloys with strong magnetic anisotropy (e.g., Co, CoFe, CoNiFe, CoNiZn, CoNiMn) can also be synthesized into high aspect-ratio fibers by the same magnetic-field-assisted solvothermal method. Supporting data (Figure S4) confirm similar morphology and anisotropic responses, demonstrating the scalability and generality of this approach.

To investigate the influence of aspect ratio on magnetic properties, micromagnetic simulations were conducted under dynamic magnetic fields for microwires with systematically varied geometries (Figure S5). At low aspect ratios ranging from 1:1 to 3:1, the nanochain exhibited uniform single-domain states, indicating that the shape anisotropy was insufficient to destabilize the simple magnetization orientation. When the aspect ratio increased to 5:1, the simulations revealed a distinct transition to radial domain orientations,[42] accompanied by pronounced magnetic domain deflection. This behavior suggests that elongated geometries promote internal demagnetizing fields and non-uniform spin distributions, which alter the equilibrium magnetic configuration. With further increases in aspect ratio, the microwires displayed increasingly complex multidomain patterns, including curling and vortex-like states, which provided enhanced responsiveness to external magnetic stimuli. The development of these intricate domain structures reflects the competition between exchange energy, magnetostatic interactions, and anisotropy energy. Importantly, the elongated geometry strengthens the effective magnetic anisotropy, thereby amplifying coercivity and magnetization stability under dynamic conditions. These results demonstrate that aspect ratio is a key parameter in tailoring both the static and dynamic magnetic responses of microwires, and that ultralong microwires with high aspect ratios hold significant promise for applications in flexible magnetic devices, spintronic components, and magnetically responsive textiles.

To validate micromagnetic simulation results, CoNi samples with varying aspect ratios were prepared by adjusting the

Please cite this article in press as: Wen et al., Programmable microwave-driven actuation systems with angle sensitivity and multimodal response, Matter (2026), https://doi.org/10.1016/j.matt.2026.103033

ethylenediamine (EDA) content, spanning from short chain to microwire configurations. Magnetic permeability was measured across the 2–18 GHz range (Figure S6). Experimental results indicated that real permeability increased with fiber length, peaking at 2 GHz for CoNi microwires before rapidly declining. Similarly, imaginary permeability also increased with fiber length, in agreement with micromagnetic simulations, which suggested that domain structures become more complex as the aspect ratio grows. This rise in imaginary permeability is attributed to enhanced eddy current effects, as longer fibers provide more surface area for domain interactions with the electromagnetic field, leading to increased energy dissipation as heat.[43] Stronger eddy currents in longer CoNi microwires result in greater heat generation, improving microwave-to-heat conversion efficiency, which is crucial for rapid thermal response applications. Simultaneously, as aspect ratio increases, Ms rises from 139.8 to 170 emu/g, and coercivity nearly doubles from 16.3 to 32.1 Oe (Figure S7), underscoring the substantial impact of shape on magnetic properties. The larger surface area in longer fibers enables more magnetic moments to align under an external field, enhancing Ms. The increase in coercivity reflects greater shape anisotropy, which hinders domain reversal and strengthens magnetic stability. This anisotropy also boosts microwave-to-heat conversion, as materials with higher aspect ratios absorb more energy and dissipate it as heat, minimizing energy loss to domain reversal. These combined effects enhance the material's performance in energy conversion applications.

These findings underscore that the ultrahigh aspect ratio imparts superior magnetic characteristics, while the highly oriented alignment and smooth microwire surfaces provide an ideal foundation for subsequent processing into woven fabrics or composites. Such structural advantages not only facilitate large-scale fabric assembly but also enable anisotropic responses under microwave fields, laying the groundwork for programmable and multimodal actuation in small-scale robotic applications.

Angle-sensitive microwave-to-heat conversion of composite fibers and fabrics

By unrolling highly anisotropic CoNi microwires and helically wrapping them at a 45° angle around silver fiber, we fabricated continuous CoNi-based magnetic fibers of virtually unlimited length (Figures 3A and 3B). This helical configuration optimizes magnetic domain alignment while simultaneously enhancing the mechanical resilience and bending compliance of the composite. The outer layer of CoNi microwires exhibited strong microwave absorption,[44] while the inner silver fiber reflected incident radiation back toward the CoNi layer, enabling reabsorption. The corresponding inner silver fiber predominantly reflects incident radiation. This cyclical absorption-reflection-reabsorption pathway markedly amplified the efficiency of microwave-to-thermal energy conversion. Under irradiation with a 2.45 GHz microwave source placed 20 cm away, the microwave intensity of 0.1 W/cm^2 (Figure 3C), the CoNi fabric demonstrated the most rapid thermal rise and the highest conversion yield compared with pure CoNi microwires and commercial carbonyl iron over a 3 min exposure, underscoring the critical role of anisotropic weaving in enhancing microwave-thermal transduction.

Using silver fiber as the weft and CoNi fiber as the warp, we further engineered a woven fabric exhibiting pronounced anisotropic conductivity and angle-sensitive microwave response. The reflection and absorption of incident electromagnetic waves clearly demonstrated this angular dependence. Firstly, electromagnetic interference (EMI) shielding[45,46] measurements of CoNi fabric (thickness = 2 mm) were performed at varying incident angles (Figure 3D; angle definition in Figure S7). The results revealed a nearly linear dependence of shielding effectiveness on angle, dominated by absorption rather than reflection, indicating distinct angle-dependent heating characteristics. When the testing angle (CoNi fabric setting angle) reached 90°, the measured EMI was as high as 78.7 dB, with the shielding effectiveness absorption (SEA) accounting for 62.7 dB.[47] Complementary infrared thermography (Figure 3E; angle definition in Figure S8) further verified this phenomenon: parallel irradiation (when microwave incidence angle $\theta_1 = 0°$) induced an ultrafast thermal response within 2 s but with limited capture, whereas increasing the incidence angle enhanced energy trapping, reaching a maximum at $\theta_1 = 60°$. The angle-sensitive response describes the anisotropic microwave absorption of the CoNi fabric, where the heating efficiency depends on the incidence angle or polarization of the microwave. These findings establish the crucial link between fabric anisotropy,[48] angular selectivity, and microwave-driven thermal dynamics.

The deep mechanism underlying this angular sensitivity is closely related to the magnetic domain dynamics and interfacial polarization[49] of oriented arrangement CoNi microwires. At first, micromagnetic simulations illuminate the underlying magnetic dynamics. As shown in Figure S11A, two parallel fibers (simulated interlayer fiber orientation angle $\theta_2 = 0°$) exhibit markedly larger domain deflections compared with a single fiber (Figure S5C), signifying a cooperative effect driven by dipole-dipole interactions that amplify the response to dynamic fields. At $\theta_2 = 45°$ stacking (Figure S11B), the system transitions from collinear to non-collinear coupling, triggering stronger dynamic excitations and the emergence of half-vortex topological defects. At $\theta_2 = 90°$ (Figure S11C), magnetic moments undergo rapid reorientation, revealing a fundamental change in coupling mechanisms: perpendicular geometries induce pronounced non-collinear dipolar interactions, dramatically lowering the energy barrier for magnetization switching. This behavior mimics a first-order magnetic phase transition, accompanied by the transient creation and annihilation of topological defects, thereby intensifying hysteresis losses and nonlinear responses. Meanwhile, as shown in Figure S12, interfacial polarization effects in bilayer CoNi fabrics became evident. By stacking fabrics at varying cross-angles, we constructed layered architectures in which charge distribution was simultaneously governed by one-dimensional fiber orientation and two-dimensional planar constraints.[50] As the interlayer alignment gradually increases from 0° to 90°, the geometric symmetry of charge distribution is reconfigured, leading to a monotonic decline in both the real and imaginary components of the dielectric constant.[51] Consequently, the angle-dependent peak absorption of microwaves can be continuously tuned across a broad range of incidence conditions.

The strong angular sensitivity endows multilayer stacked films with versatile absorption and thermal conversion capabilities.

Please cite this article in press as: Wen et al., Programmable microwave-driven actuation systems with angle sensitivity and multimodal response, Matter (2026), https://doi.org/10.1016/j.matt.2026.103033

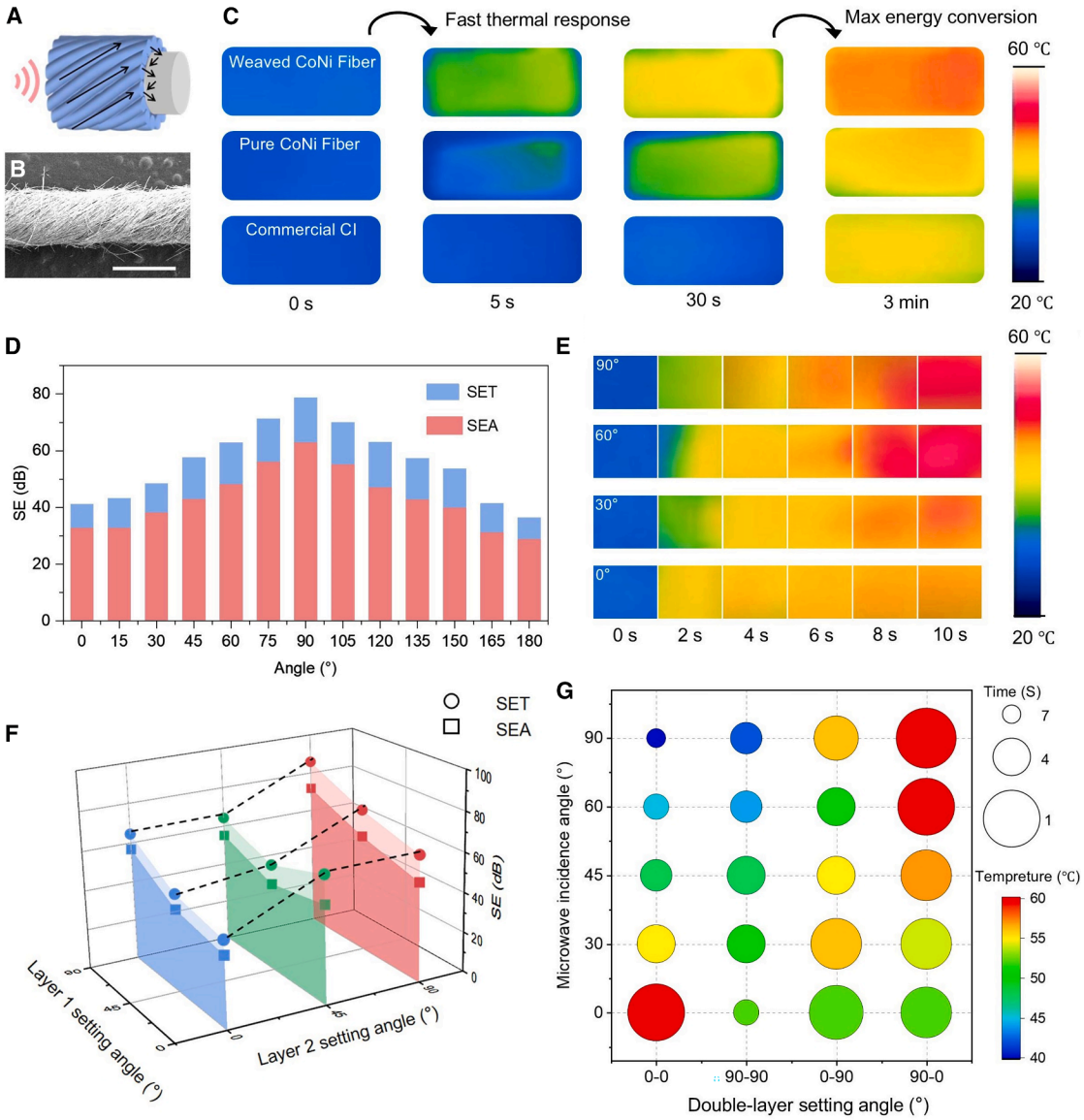

Figure 3. The angle sensitivity of CoNi fabric

(A) Principle of enhanced electromagnetic wave absorption through winding technique.

(B) SEM image of CoNi thread wound at a 45° angle, scale bar, 1mm.

(C) Infrared imaging showing microwave-heat conversion for CoNi fabric compared to pure CoNi microwires and commercial CI under microwave irradiation.

(D) EMI shielding effectiveness of single-layer CoNi fabric at various testing angles.

(E) Infrared imaging of microwave-heat conversion for single-layer CoNi fabric under different microwave exposures angles.

(F) EMI shielding effectiveness of double-layer CoNi fabric at various testing angles.

(G) The temperature and response time (defined as the time to reach 40°C) for microwave-to-heat conversion in double-layer CoNi fabric were measured under various microwave incidence angles and double-layer CoNi fabric setting angles.

Figures 3F and S13 illustrate a bilayer stacking strategy to achieve omnidirectional absorption. Considering the angular modulation of microwave-thermal conversion, rotating two CoNi fabric (thickness = 1 mm each) layers at distinct orientations yields shielding comparable to a single layer, confirming that multilayer assembly introduces no performance trade-off. The measured EMI of 90–90 was up to 85.9 dB, with the SEA accounting for 71.8 dB. More strikingly, in Figures 3G and S14, vertical stacking (0–90 and 90–0) enhances conversion efficiency across varying incidence angles while suppressing disparities in response speed thereby achieving a comprehensive improvement. This refined control over thermal conversion by layer orientation and angular design provides a conceptual foundation for multifunctional applications—for example, robotic grippers capable of executing distinct mechanical tasks under identical microwave stimuli.

Please cite this article in press as: Wen et al., Programmable microwave-driven actuation systems with angle sensitivity and multimodal response, Matter (2026), https://doi.org/10.1016/j.matt.2026.103033

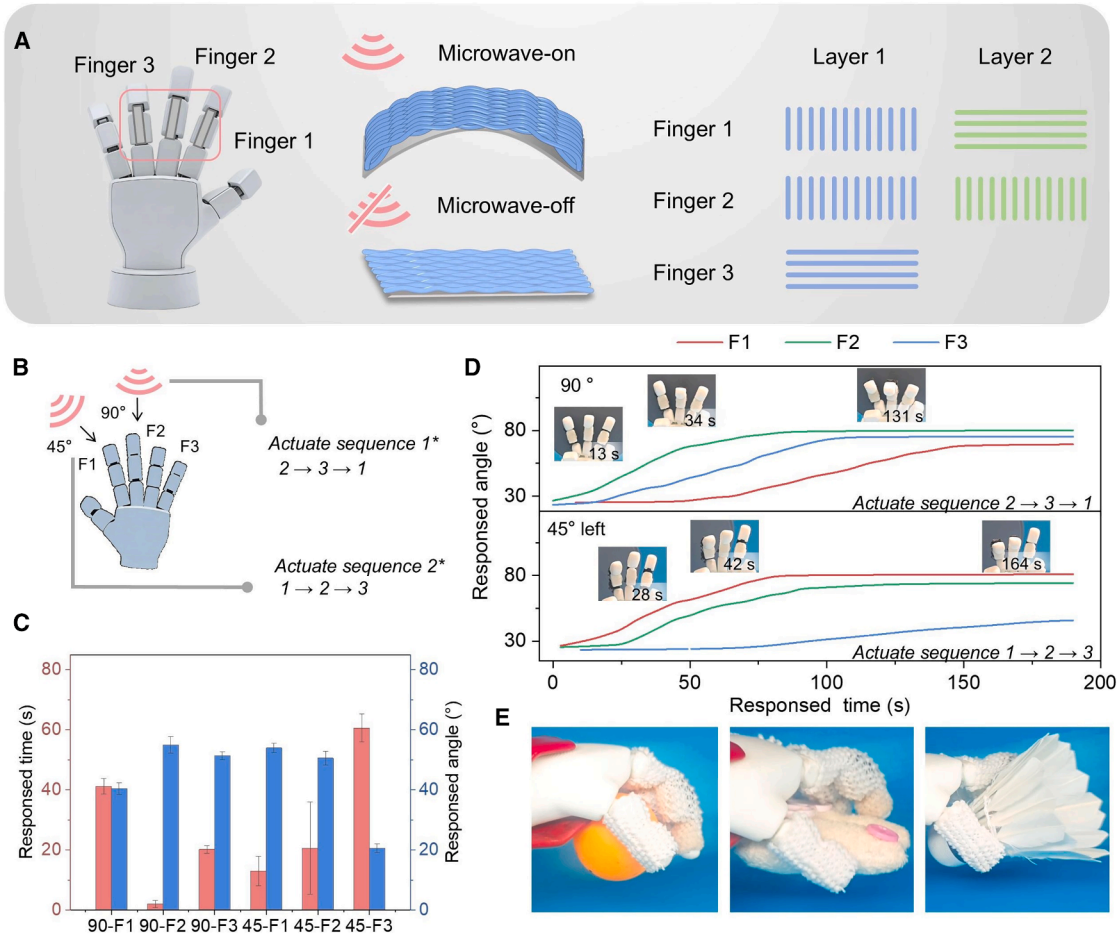

Figure 4. Dynamic behavior of the robotic hand with sequential and multimodal response

(A) Schematic illustration of the robotic hand's structural design, joint actuation performance, and CoNi fabric arrangement at distinct finger joints.

(B) Schematic of the sequential bending sequence of robotic fingers under microwave irradiation at different incident angles.

(C) Bending time and bending angle of individual robotic fingers under microwave irradiation at different incident angles.

(D and E) Demonstration of the robotic hand grasping various objects.

Microwave-driven programmable multimodal robotic actuation

The conventional photonic and magnetic actuation strategies face inherent limitations in penetration, hardware footprint, or miniaturization compatibility. Though microwaves enable deeply penetrating, antenna-free remote actuation across diverse materials, selective and sequentially programmable actuation via this stimulus remains an unsolved challenge.[37] In our novel design system, the angle sensitivity of CoNi fabric is leveraged to achieve material-level encoding for sequential control.

Specifically, by utilizing the fabric's intrinsic angle-dependent microwave absorption and thermal conversion, we developed an angle-sensitive, microwave-driven robotic hand. Material-level encoding through stacked CoNi fabrics with predefined orientations enables directional microwave irradiation to trigger differentiated thermal responses, facilitating programmed sequential actuation of the robotic fingers under fixed microwave exposure. To achieve sequential actuation, each of the three robotic finger joints is integrated with a CoNi fabric/SMA composite actuator, each possessing distinct layer configurations. The fabric's angle-sensitive microwave response is fully retained after integration into the robotic system. Mechanistically, the CoNi fabric/SMA heterostructure preserves the anisotropic microwave absorption of the aligned CoNi microwires, generating angle-dependent differential thermal energy via stable magnetic domain dynamics, which drives reversible phase transitions in the SMA and subsequent actuation of the robotic fingers.[52]

To achieve programmable shape transformation of the robotic hand, we employed the fabric's intrinsic angle-dependent microwave absorption and thermal conversion, integrating CoNi fabrics with SMAs (transition temperatures: 40°C–60°C). Material-level encoding through stacked CoNi fabrics with predefined orientations enables directional microwave irradiation to trigger differentiated thermal responses, facilitating sequential actuation of the robotic fingers under fixed microwave exposure. As shown in Figure 4A, three distinct fabric architectures were applied to the robotic fingers: finger 1 with two vertically stacked layers, finger 2 with two parallel layers, and finger 3 with a single

Please cite this article in press as: Wen et al., Programmable microwave-driven actuation systems with angle sensitivity and multimodal response, Matter (2026), https://doi.org/10.1016/j.matt.2026.103033

layer. When irradiated with 2.45 GHz microwaves at a 90° incident angle (20 cm distance), finger 2 responded first, followed by finger 1, and then finger 3, creating a sequential actuation order of 2→1→3. Shifting the microwave incident angle to 45° from the left reversed the order to 1→2→3 (Figure 4B; Video S1), and similar behavior was observed with 45° irradiation from the right in Figure S15, with only a slight increase in response time. These results confirm that the incident angle, not the microwave distance, determines the actuation sequence. Figure 4C demonstrates the stability and precision of the CoNi fabric's angle-controlled response. The motion trajectories of the individual fingers are shown in Figures 4D and S16. At a 45° incident angle, finger 1 driven by enhanced non-collinear dipolar coupling and interfacial polarization between orthogonally oriented microwire layers, triggering rapid SMA phase transitions and immediate actuation. Finger 2, with parallel-stacked CoNi bilayers, bends through cumulative thermal energy under this angle. Finger 3, with a single CoNi layer perpendicular to the microwave, undergoes delayed actuation due to reduced microwave-to-heat conversion. Conversely, 90° irradiation maximizes absorption efficiency in Finger 2, reversing the actuation order.

To further demonstrate the practical utility of the actuation strategy for object manipulation, we evaluated the grasping performance of the robotic hand. As shown in Figure 4E and Video S2, the robotic hand successfully grasped objects of diverse geometries (spherical and irregular shapes) and material compositions (plastic, knitted fabric, and feather). This demonstration validates the translational applicability of the angle-programmable actuation mechanism beyond basic motion regulation, substantially expanding the functional scope of the small-scale robotic system. Beyond object manipulation, we further examined whether the same materials-encoded actuation strategy could be retained in a reduced-size bending prototype. Notably, this design strategy exhibits excellent scalability and applicability at reduced dimensions: a millimeter-scale bending robot (3×10 mm) fabricated with the same fabric stacking configurations (90–0, 90–90, 90) achieves diverse actuation modes including fully relaxed, semi-relaxed, and slightly bent states under 2.45 GHz microwave irradiation (Figure S17), with the corresponding infrared images (Figure S17B) revealing distinct thermal responses across different regions, further confirming the effectiveness of our angle-sensitive actuation design at smaller scales. Practically, leveraging this angle-sensitive mechanism, microwave signal modulation enables independent, site-selective actuation via tuning key parameters, fully embodying the cross-scale intrinsic programmability of our CoNi-SMA system.

Microwave-driven walking robot

Prior validation confirmed the feasibility of material-encoded programmable actuation for our anisotropic CoNi fabric. To further unlock its robotics application potential, we fabricated a microwave-driven walking robot, where tether-free, remotely actuated locomotion relevant to operation in unstructured, confined environments is achieved via an elastic leg design with anisotropic friction (Figure 5A). The core actuation mechanism of this design stems from the CoNi fabric's highly efficient microwave-to-thermal conversion: microwave activation triggers localized heating and SMA-induced leg bending for rear foot sliding and front foot locking via anisotropic friction. While deactivation drives cooling-induced SMA recovery for hind leg locking and foreleg forward sliding (Figures 5B and 5C).

CoNi fabric's intrinsic angle sensitivity also critically governs the walking robot's locomotion speed. Consistent with robotic hand, varying microwave incident angles induce differential thermal responses, thus modulating the bending angle and actuation rate of the SMA. As shown in Figure 5D, this inherent angle-dependent thermal characteristic enables precise, continuous tuning of the robot's locomotion speed solely by adjusting the microwave incident angle. Specifically, a maximum locomotion speed of 16 body lengths per hour (BL/h) is achieved under the most common normal top microwave incidence, while the speed drops to 14 BL/h and 4 BL/h under side and front microwave incidence (Figure 5E; Video S3). More importantly, in Figure 5F, repeated bending-recovery cycles under continuous 2.45 GHz microwave on-off stimulation validate the mechanical robustness[53] of the robotic platform. Even after prolonged cyclic operation, the CoNi fabric maintains consistent and stable thermal output to the SMA actuator, enabling highly repeatable shape deformation without observable performance degradation. A slight temporal delay is observed between the microwave on-off pulses and the actuator's bending deformation, as documented in Figure S18. This minor delay effectively buffers the actuation process, resulting in smoother locomotion sequences and reduced instantaneous mechanical stress on the robotic structure during cyclic actuation.

To demonstrate the environmental adaptability of walking robot, we present full continuous walking sequences across varied substrates and inclination angles (Figure 5G). Under a microwave power density of 0.4 W/cm^2, the robot realizes repeated locomotion on painted wood, PVC, and cardboard even with tilted surfaces up to 10°, with Videos S4 and S5 verifying its repeatable smooth cyclic walking. This multi-environment adaptability stems from high-efficiency microwave convert, sufficient SMA driving force and excellent overall structural stability.

Collectively, these results verify that the integrated CoNi-SMA system features structural durability and repeatable, controllable actuation kinetics. The synergy of robust mechanical design, stable thermal conversion, and predictable actuation timing ensures consistent motion under prolonged repeated microwave exposure, enabling reliable operation in controlled and representative unstructured settings, while its inherent scalability and modularity support adaptation to diverse applications. Potential application extensions of this system include microwave-controlled rescue robots remote reconnaissance microrobots for enclosed or hazardous spaces. Altogether, the integration of structural durability, programmable actuation, and environmental adaptability establishes a versatile foundation for next-generation autonomous micro-robotic systems powered by uniform, remotely delivered microwave stimuli.

Conclusion

In this work, we demonstrated a series of strategies for a microwave-driven strategy for small-scale robotic actuation, integrating CoNi fabrics with SMAs to realize programmable and multifunctional responses. By configuring the orientation and layering of CoNi fabrics, sequential regional actuation can be triggered by a

Please cite this article in press as: Wen et al., Programmable microwave-driven actuation systems with angle sensitivity and multimodal response, Matter (2026), https://doi.org/10.1016/j.matt.2026.103033

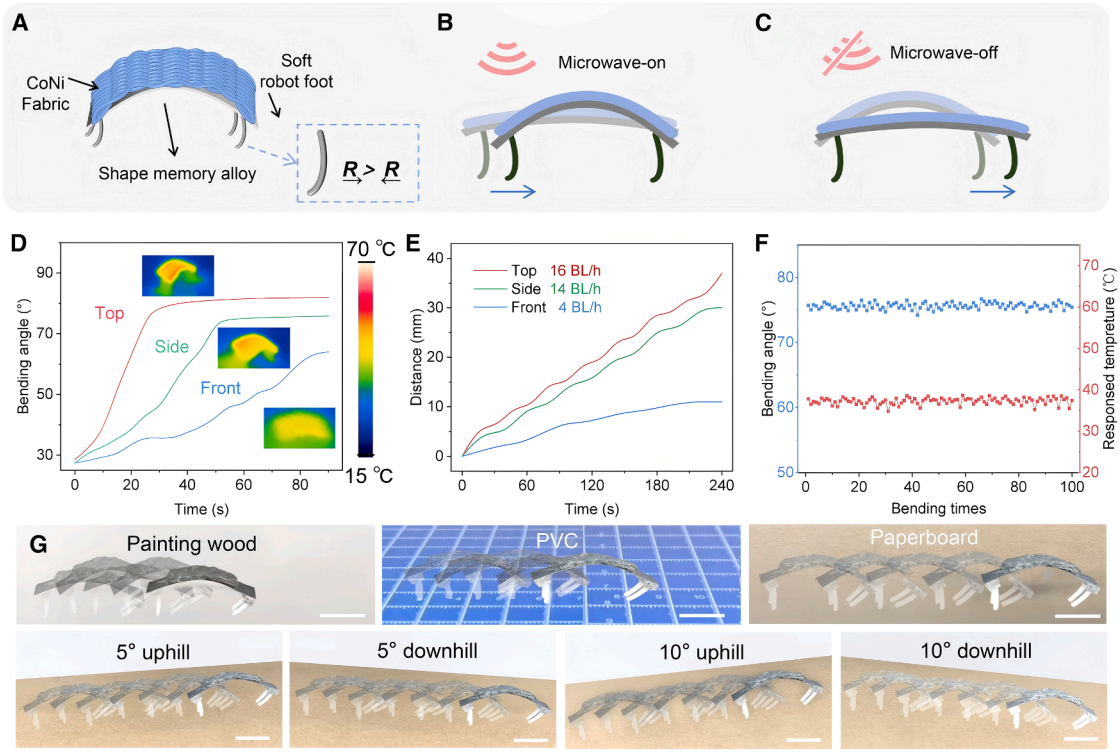

Figure 5. Operation and dynamic behavior of the CoNi fabric-based walking robot under microwave control

(A) Diagram of the walking robot structure.

(B and C) Demonstration of the robot's movement mechanism under (B) microwave-on and (C) microwave-off, resulting in movement in the indicated direction.

(D) The responsive temperature of the CoNi fabric in the CoNi fabric-SMA composite system, and the corresponding time-dependent bending angle of the SMA actuator under microwave irradiation at different incident angles.

(E) Locomotion speed of the walking robot under microwave irradiation at different incident angles.

(F) Stability of the temperature and bending angle response under cyclic microwave on-off switching.

(G) Sequential photographs of the robot's locomotion across substrates with different surface properties and at different incline angles under consecutive microwave on-off cycles. Scale bars, 1 cm.

single microwave signal, enabling robots to perform multiple distinct actions without the need for complex control systems. Moreover, the system's antenna-free passive design improves operational reliability and simplifies manufacturing. Our robotic hand and walking robot validate the programmable actuation and broad applicability of the CoNi fabric+SMA system, while this work unlocks the unique potential of microwave wireless actuation for microrobotics and provides a material-driven technical pathway toward multifunctional autonomous small-scale robot for complex extreme environments.

METHODS

Chemicals

Cobalt acetate tetrahydrate ($Co(CH_3COO)_2 \cdot 4H_2O$) and nickel acetate tetrahydrate ($Ni(CH_3COO)_2 \cdot 4H_2O$) were purchased from Shanghai Aladdin Reagent Co., Ltd. Ethylenediamine ($C_2H_4(NH_2)_2$), polyethylene glycol ($H(OCH_2CH_2)nOH$ 2000, PEG 2000), sodium hydroxide (NaOH), ethylene glycol ($HOCH_2$-CH_2OH, EG), and other reagents were obtained from Sinopharm Chemical Reagent Co., Ltd. Deionized water (DI water) was prepared using a Milli-Q system.

Synthesis of CoNi microwire

CoNi microwires were synthesized using a typical solvothermal method. Initially, 3.2 mmol of $Co(CH_3COO)_2 \cdot 4H_2O$ and 0.8 mmol of $Ni(CH_3COO)_2 \cdot 4H_2O$ were used as metal precursors. In addition, 3.2 M NaOH was introduced as an alkaline regulator, while 13 mL of $C_2H_4(NH_2)_2$ served as a complexing agent, and 0.5 g of polyethylene glycol (PEG 2000) was added as a dispersing agent to enhance homogeneity. The mixture was dissolved in 40 mL of ethylene glycol and stirred at 65°C until homogeneous. Subsequently, the solution was transferred to a 100 mL stainless steel autoclave lined with PTFE and subjected to hydrothermal reaction at 200°C for 20 h. During this process, magnets were attached to the sides of the reactor to orient microwire growth. The product was washed multiple times with DI water and ethanol to eliminate residues and surface adsorbates, then reduced for 1 h at 800°C in 5% H_2/Ar atmosphere.

Fabrication of winded CoNi microwires

The oriented CoNi microwires were separated into bundles and wound clockwise around silver fiber, maintaining constant tension to ensure tight winding. This process was repeated to produce the winded CoNi thread.

Fabrication of oriented CoNi fabric

Using a loom, the CoNi threads were woven into a flexible fabric. Specifically, silver fibers were secured as warp threads, while the oriented CoNi threads were integrated to create the CoNi fabric.

Fabrication of microwave-controllable robotic hand

The main body of the robotic hand was fabricated via fused deposition modeling (FDM) 3D printing using a Bambu Lab ×1 Carbon 3D printer with Bambu PLA Basic filament, and the structural model was obtained from an open-source online repository. The as-prepared oriented CoNi fabrics were tailored into 1 × 2.5 cm rectangular specimens, with the aligned CoNi microwires oriented either along the long axis or the short axis of the rectangle to enable parallel or perpendicular fiber alignment between two stacked fabric layers. The CoNi fabrics with designed stacking configurations were then integrated onto the surface of SMA sheets to construct the actuating units. A polydimethylsiloxane (PDMS) precursor solution (Sylgard 184, Dow Corning Inc.) was prepared by mixing the curing agent and base monomer at a mass ratio of 1:10. The CoNi fabric assemblies were immersed in the PDMS precursor solution for 10 min, and then firmly attached to the SMA sheets. The assembled samples were placed in a vacuum chamber for 3 min to remove residual air bubbles, followed by curing at room temperature for 6 h. The both side of integrated CoNi fabric-SMA actuating units were trimmed into a wedge shape at both ends and inserted into the joints of the 3D-printed finger structures to form microwave-controllable articulations. Finally, all fingers of the robotic hand were wrapped with a layer of white knitted mesh to enhance structural integrity and surface friction during grasping.

Fabrication of microwave-driven walking robot

The actuating unit of the walking robot was fabricated following the aforementioned PDMS encapsulation protocol, with a single layer of the as-prepared CoNi fabric integrated onto the SMA sheet. Four elastic robot feet were fabricated via mold casting using a UV-curable flexible polyurethane (PU) elastomer resin, then securely attached to the bottom surface of the SMA-based actuating unit. The contact angle between each elastic foot and the substrate was finely adjusted to ensure complete consistency across all four feet.

Materials characterization

The crystalline phases of the samples were characterized using a Bruker-Axe X-ray diffractometer equipped with a Cu Kα radiation source (λ = 1.5406 Å, 40 kV, 40 mA). The surface morphology and structural features were investigated using a Hitachi S-4800 field-emission scanning electron microscope (FE-SEM) combined with EDS mapping. Detailed structural and crystallographic data were obtained through a JEOL JEM-2100 F field-emission TEM. XPS measurements were conducted using a Thermo Scientific ESCALAB 250Xi instrument with a monochromatic X-ray source. Magnetic hysteresis loops were evaluated with a superconducting quantum interference device magnetometer (MPMS(SQUID) VSM).

Micromagnetic simulation method

The magnetization configuration was simulated by MuMax3.10. The magnetic parameters of the different structure are shown in the following texts. The micromagnetic exchange constant A = 13.2 × 10^{-12} J/m, and the saturation magnetization Ms are collected from VSM results. Alpha = 0.01. Dynamic magnetic fields = 0.013×sin(2×pi×8e9×t) T.

RESOURCE AVAILABILITY

Lead contact

Requests for further information, resources, and materials should be directed to and will be fulfilled by the lead contact, Wenbin You (wbyou@fudan.edu.cn).

Materials availability

This study did not generate new unique reagents.

Data and code availability

Any additional information required to reanalyze the data reported in this paper is available from the lead contact upon request.

ACKNOWLEDGMENTS

M.W., J.C., and Y.W. contributed equally to this work. This work was supported by the National Natural Science Foundation of China (nos. 12327804, 52231007, T2321003, 22088101, and 22405050), the National Key Research Program of China (nos. 2024YFA1208902, 2024YFA1408000, and 2021YFA1200600), the Science and Technology Commission of Shanghai Municipality (no. 24ZR1406400), and Shanghai Municipal Education Commission (no. 24KXZNA06).

AUTHOR CONTRIBUTIONS

Conceptualization, R.C. and W.Y.; methodology, M.W. and W.Y.; investigation, M.W., Y.W., C.Z., X.L., X.X., Z.Y., and J.W.; formal analysis, M.W., Y.W., J.Q., and Z.Y.; data curation, G.L., J.Q., and Z.Y.; visualization, M.W. and X.L.; writing – original draft, M.W.; writing – review and editing, M.W., R.C., and W.Y.; supervision, R.C., W.Y., and J.C.

DECLARATION OF INTERESTS

The authors declare no conflict of interest.

DECLARATION OF GENERATIVE AI AND AI-ASSISTED TECHNOLOGIES IN THE WRITING PROCESS

During the preparation of this work, the authors used Gemini to polish linguistic phrasing. After utilizing this tool, the authors reviewed and edited the content as needed and bear full responsibility for all material in this publication.

SUPPLEMENTAL INFORMATION

Supplemental information can be found online at https://doi.org/10.1016/j.matt.2026.103033.

Received: September 30, 2025
Revised: May 15, 2026
Accepted: August 28, 2026

REFERENCES

1. Bo, R., Xu, S., Yang, Y., and Zhang, Y. (2023). Mechanically-guided 3D assembly for architected flexible electronics. Chem. Rev. *123*, 11137–11189. https://doi.org/10.1021/acs.chemrev.3c00335.

Please cite this article in press as: Wen et al., Programmable microwave-driven actuation systems with angle sensitivity and multimodal response, Matter (2026), https://doi.org/10.1016/j.matt.2026.103033

2. Yang, Y., and Gao, W. (2019). Wearable and flexible electronics for continuous molecular monitoring. Chem. Soc. Rev. *48*, 1465–1491. https://doi.org/10.1039/c7cs00730b.

3. Hui, Z., Zhang, L., Ren, G., Sun, G., Yu, H.D., and Huang, W. (2023). Green flexible electronics: natural materials, fabrication, and applications. Adv. Mater. *35*, 2211202. https://doi.org/10.1002/adma.202211202.

4. Chen, Z., Chen, J., Jung, S., Kim, H.Y., Lo Preti, M., Laschi, C., Ren, Z., Sitti, M., Full, R.J., and Yang, G.Z. (2025). Bioinspired and biohybrid soft robots: Principles and emerging technologies. Matter *8*, 102045. https://doi.org/10.1016/j.matt.2025.102045.

5. Tang, L., Wang, L., Yang, X., Feng, Y., Li, Y., and Feng, W. (2021). Poly (N-isopropylacrylamide)-based smart hydrogels: Design, properties and applications. Prog. Mater. Sci. *115*, 100702. https://doi.org/10.1016/j.pmatsci.2020.100702.

6. Gardan, J. (2019). Smart materials in additive manufacturing: state of the art and trends. Virtual Phys. Prototyp. *14*, 1–18. https://doi.org/10.1080/17452759.2018.1518016.

7. Chen, Y., Valenzuela, C., Liu, Y., Yang, X., Yang, Y., Zhang, X., Ma, S., Bi, R., Wang, L., and Feng, W. (2025). Biomimetic artificial neuromuscular fiber bundles with built-in adaptive feedback. Matter *8*, 101904. https://doi.org/10.1016/j.matt.2024.10.022.

8. Yang, L., Liu, Y., Bi, R., Chen, Y., Valenzuela, C., Yang, Y., Liu, H., Wang, L., and Feng, W. (2025). Direct-Ink-Written Shape-Programmable Micro-Supercapacitors with Electrothermal Liquid Crystal Elastomers. Adv. Funct. Mater. *35*, 2504979. https://doi.org/10.1002/adfm.202504979.

9. Han, K., and Snezhko, A. (2025). Field-Driven Out-of-Equilibrium Collective Patterns for Swarm Micro-Robotics. ACS Nano *19*, 16248–16266. https://doi.org/10.1021/acsnano.5c01238.

10. Zhu, D., Lu, J., Zheng, M., Wang, D., Wang, J., Liu, Y., Wang, X., and Zhang, M. (2023). Self-powered bionic antenna based on triboelectric nanogenerator for micro-robotic tactile sensing. Nano Energy *114*, 108644. https://doi.org/10.1016/j.nanoen.2023.108644.

11. Tasoglu, S., Diller, E., Guven, S., Sitti, M., and Demirci, U. (2014). Untethered micro-robotic coding of three-dimensional material composition. Nat. Commun. *5*, 3124. https://doi.org/10.1038/ncomms4124.

12. Luo, R.C., and Kuo, C.W. (2016). Intelligent seven-DoF robot with dynamic obstacle avoidance and 3-D object recognition for industrial cyber–physical systems in manufacturing automation. Proc. IEEE *104*, 1102–1113. https://doi.org/10.1109/jproc.2015.2508598.

13. Zhang, D., Ren, Y., Barbot, A., Seichepine, F., Lo, B., Ma, Z.C., and Yang, G.Z. (2022). Fabrication and optical manipulation of micro-robots for biomedical applications. Matter *5*, 3135–3160. https://doi.org/10.1016/j.matt.2022.07.003.

14. Gupta, B., Goudeau, B., and Kuhn, A. (2017). Wireless electrochemical actuation of conducting polymers. Angew. Chem. Int. Ed. *56*, 14183–14186. https://doi.org/10.1002/anie.201709038.

15. Dong, Y., Wang, J., Guo, X., Yang, S., Ozen, M.O., Chen, P., Liu, X., Du, W., Xiao, F., Demirci, U., and Liu, B.F. (2019). Multi-stimuli-responsive programmable biomimetic actuator. Nat. Commun. *10*, 4087. https://doi.org/10.1038/s41467-019-12044-5.

16. Sun, L., Zhao, Q., Che, L., Li, M., Leng, X., Long, Y., and Lu, Y. (2024). Multi-Stimuli-Responsive Weldable Bilayer Actuator with Programmable Patterns and 3D Shapes. Adv. Funct. Mater. *34*, 2311398. https://doi.org/10.1002/adfm.202311398.

17. Han, B., Zhang, Y.L., Chen, Q.D., and Sun, H.B. (2018). Carbon-based photothermal actuators. Adv. Funct. Mater. *28*, 1802235. https://doi.org/10.1002/adfm.201802235.

18. Chen, J., Cao, Y., Pei, J., and Zhao, H. (2023). Multifunctional actuator based on graphene/PDMS composite materials with shape programmable configuration and high photothermal conversion capability. ACS Appl. Mater. Interfaces *15*, 31917–31926. https://doi.org/10.1021/acsami.3c06041.

19. Wang, F., Bi, R., Chen, Y., Yang, Y., Liu, Y., Yang, L., Shen, Y., Wang, L., and Feng, W. (2025). 4D printing of carbon-fiber-reinforced liquid crystal elastomers for self-deployable solar panels. Mater. Horiz. *12*, 5315–5324. https://doi.org/10.1039/d5mh00363f.

20. Zhao, J., Lu, T., Zhang, Y., Zhang, C., Pan, C., Tan, Y., Zhu, J., Li, B., Zhang, L., Shi, M., and Li, X. (2023). Magnetically actuated adhesives with switchable adhesion. Adv. Funct. Mater. *33*, 2305484. https://doi.org/10.1002/adfm.202305484.

21. Wang, S., Luo, H., Linghu, C., and Song, J. (2021). Elastic energy storage enabled magnetically actuated, octopus-inspired smart adhesive. Adv. Funct. Mater. *31*, 2009217. https://doi.org/10.1002/adfm.202009217.

22. Linghu, C., Wang, C., Cen, N., Wu, J., Lai, Z., and Song, J. (2018). Rapidly tunable and highly reversible bio-inspired dry adhesion for transfer printing in air and a vacuum. Soft Matter *15*, 30–37. https://doi.org/10.1039/c8sm01996g.

23. Hamedi, M.M., Campbell, V.E., Rothemund, P., Güder, F., Christodouleas, D.C., Bloch, J.F., and Whitesides, G.M. (2016). Electrically activated paper actuators. Adv. Funct. Mater. *26*, 2446–2453. https://doi.org/10.1002/adfm.201505123.

24. Carpi, F., Kornbluh, R., Sommer-Larsen, P., and Alici, G. (2011). Electroactive polymer actuators as artificial muscles: are they ready for bioinspired applications? Bioinspiration Biomimetics *6*, 045006. https://doi.org/10.1088/1748-3182/6/4/045006.

25. Belding, L., Baytekin, B., Baytekin, H.T., Rothemund, P., Verma, M.S., Nemiroski, A., Sameoto, D., Grzybowski, B.A., and Whitesides, G.M. (2018). Slit tubes for semisoft pneumatic actuators. Adv. Mater. *30*, 1704446. https://doi.org/10.1002/adma.201704446.

26. Li, Z., Ye, Z., Han, L., Fan, Q., Wu, C., Ding, D., Xin, H.L., Myung, N.V., and Yin, Y. (2021). Polarization-modulated multidirectional photothermal actuators. Adv. Mater. *33*, 2006367. https://doi.org/10.1002/adma.202006367.

27. Zhao, J., Li, X., Tan, Y., Liu, X., Lu, T., and Shi, M. (2022). Smart adhesives via magnetic actuation. Adv. Mater. *34*, 2107748. https://doi.org/10.1002/adma.202107748.

28. Su, J.L., Cai, Z.X., Mao, Y., Chen, L., Yu, X.Y., Yu, Z.C., Ma, Q., Huang, S.Q., Zhang, J., You, J.W., and Cui, T.J. (2025). Multi-Dimensional Multiplexed Metasurface for Multifunctional Near-Field Modulation by Physics-Driven Intelligent Design. Adv. Sci. *12*, 2503899. https://doi.org/10.1002/advs.202503899.

29. Feng, H., Bu, L., Ling, Y., Jiang, S., Zhao, X., Li, Z., Xu, M., Xu, S., and Wang, X. (2025). A Heterogeneous Cascaded Resonant MEMS Energy Harvester with In Situ Integrated PVDF Films for Sub-10 Hz Ultra-Low-Frequency Vibration Energy Harvesting. Small *21*, 2504771. https://doi.org/10.1002/smll.202504771.

30. Acosta, J.N., Falcone, G.J., Rajpurkar, P., and Topol, E.J. (2022). Multimodal biomedical AI. Nat. Med. *28*, 1773–1784. https://doi.org/10.1038/s41591-022-01981-2.

31. Wang, X., Ji, H., Gao, L., Hao, R., Shi, Y., Yang, J., Hao, Y., and Chen, J. (2024). Wearable hydrogel-based health monitoring systems: A new paradigm for health monitoring? Chem. Eng. J. *495*, 153382. https://doi.org/10.1016/j.cej.2024.153382.

32. Yang, J., Tian, X., Fan, J., Zhang, B., Li, Z., Liu, S., Xu, Z., Qin, G., and Chen, Q. (2023). Extreme condition-resistant flexible triboelectric nanogenerator and sensor based on swollen-yet-enhanced and self-healing deep eutectic gel. Polymer *283*, 126238. https://doi.org/10.1016/j.polymer.2023.126238.

33. Ma, S., Xue, P., Valenzuela, C., Liu, Y., Chen, Y., Feng, Y., Bi, R., Yang, X., Yang, Y., Sun, C., et al. (2025). 4D-Printed Adaptive and Programmable Shape-Morphing Batteries. Adv. Mater. *37*, 202505018. https://doi.org/10.1002/adma.202505018.

34. Wu, Y., Zhang, S., Yang, Y., Li, Z., Wei, Y., and Ji, Y. (2022). Locally controllable magnetic soft actuators with reprogrammable contraction-derived motions. Sci. Adv. *8*, eabo6021. https://doi.org/10.1126/sciadv.abo6021.

Please cite this article in press as: Wen et al., Programmable microwave-driven actuation systems with angle sensitivity and multimodal response, Matter (2026), https://doi.org/10.1016/j.matt.2026.103033

35. Liang, L., Yang, X., Li, C., Yu, R., Zhang, B., Yang, Y., and Ji, G. (2024). MXene-Enabled Pneumatic Multiscale Shape Morphing for Adaptive, Programmable and Multimodal Radar-infrared Compatible Camouflage. Adv. Mater. *36*, 2313939. https://doi.org/10.1002/adma.202313939.

36. Li, D., Liu, C., Yang, Y., Wang, L., and Shen, Y. (2020). Micro-rocket robot with all-optic actuating and tracking in blood. Light Sci. Appl. *9*, 84. https://doi.org/10.1038/s41377-020-0323-y.

37. Palagi, S., Mark, A.G., Reigh, S.Y., Melde, K., Qiu, T., Zeng, H., Parmeggiani, C., Martella, D., Sanchez-Castillo, A., Kapernaum, N., et al. (2016). Structured light enables biomimetic swimming and versatile locomotion of photoresponsive soft microrobots. Nat. Mater. *15*, 647–653. https://doi.org/10.1038/nmat4569.

38. Liu, Y., Wei, X., He, X., Yao, J., Tan, R., Chen, P., Yao, B., Zhou, J., and Yao, Z. (2023). Multifunctional shape memory composites for joule heating, self-healing, and highly efficient microwave absorption. Adv. Funct. Mater. *33*, 2211352. https://doi.org/10.1002/adfm.202211352.

39. Li, Y., Wu, J., Yang, P., Song, L., Wang, J., Xing, Z., and Zhao, J. (2022). Multi-Degree-of-Freedom Robots Powered and Controlled by Microwaves. Matter *9*, 2203305. https://doi.org/10.1002/advs.202203305.

40. Rao, L., Liu, Z., Wang, L., You, W., Yang, C., Zhang, R., Xiong, X., Yang, L., Zhang, H., Zhang, J., et al. (2023). Dimensional engineering of hierarchical nanopagodas for customizing cross-scale magnetic coupling networks to enhance electromagnetic wave absorption. Adv. Funct. Mater. *33*, 2306984. https://doi.org/10.1002/adfm.202306984.

41. Liu, Q., Cao, Q., Bi, H., Liang, C., Yuan, K., She, W., Yang, Y., and Che, R. (2016). CoNi@ SiO_2@ TiO_2 and CoNi@ Air@ TiO_2 microspheres with strong wideband microwave absorption. Adv. Mater. *28*, 486–490. https://doi.org/10.1002/adma.201503149.

42. Chen, Y., Wang, L., Wang, W., and Cao, M. (2017). Enhanced photoelectrochemical properties of ZnO/ZnSe/CdSe/Cu_{2-x}Se core-shell nanowire arrays fabricated by ion-replacement method. Appl. Catal. B Environ. *209*, 110–117. https://doi.org/10.1016/j.apcatb.2017.02.049.

43. Pang, H., Duan, Y., Huang, L., Song, L., Liu, J., Zhang, T., Yang, X., Liu, J., Ma, X., Di, J., and Liu, X. (2021). Research advances in composition, structure and mechanisms of microwave absorbing materials. Compos. B Eng. *224*, 109173. https://doi.org/10.1016/j.compositesb.2021.109173.

44. Pan, F., Pei, K., Chen, G., Guo, H., Jiang, H., Che, R., and Lu, W. (2023). Integrated electromagnetic device with on-off heterointerface for intelligent switching between wave-absorption and wave-transmission. Adv. Funct. Mater. *33*, 2306599. https://doi.org/10.1002/adfm.202306599.

45. Zhou, L., Hu, P., Bai, M., Leng, N., Cai, B., Peng, H.L., Zhao, P.Y., Guo, Y., He, M., Wang, G.S., and Gu, J. (2025). Harnessing the electronic spin states of single atoms for precise electromagnetic modulation. Adv. Mater. *37*, 2418321. https://doi.org/10.1002/adma.202418321.

46. Wen, J., Liu, Y., Hui, S., Deng, L., Zhang, L., Fan, X., Chen, Q., Liu, X., Li, X., Yan, N., and Wu, H. (2025). Lattice compressive strain-controlled electromagnetic wave absorption in TMDs by plasma-assisted rapid annealing. Matter *8*, 102151. https://doi.org/10.1016/j.matt.2025.102151.

47. Li, Y., Wang, Y., Li, Z., Ma, S., Zhang, Y., Fan, F., and Huang, Y. (2025). Meter-Scale Wearable Multifunctional Core-Shell Nanofiber Textiles for Ultra-Broadband Electromagnetic Interference Shielding and Infrared Stealth. Adv. Mater. *37*, 2501485. https://doi.org/10.1002/adma.202501485.

48. Xu, C., Luo, K., Du, Y., Zhang, H., Lv, X., Lv, H., Zhang, R., Zhang, C., Zhang, J., and Che, R. (2023). Anisotropic interfaces support the confined growth of magnetic nanometer-sized heterostructures for electromagnetic wave absorption. Adv. Funct. Mater. *33*, 2307529. https://doi.org/10.1002/adfm.202307529.

49. Xu, C., Xiong, X., Du, Y., Lv, X., Wu, Z., Luo, K., Qian, Y., and Che, R. (2025). Dual-coupling networks engineering of self-assembled ferromagnetic microspheres with enhanced interfacial polarization and magnetic interaction for microwave absorption. InfoMat *7*, e12645. https://doi.org/10.1002/inf2.12645.

50. Song, J., Jiao, J., Liu, H., Qi, Z., Yang, J., Ai, Y., Zhou, Y., and Wang, Y. (2025). Effect of surface state of SiC fibers on their interfacial properties. Compos. Commun. *53*, 102232. https://doi.org/10.1016/j.coco.2024.102232.

51. Sun, H., Che, R., You, X., Jiang, Y., Yang, Z., Deng, J., Qiu, L., and Peng, H. (2014). Cross-stacking aligned carbon-nanotube films to tune microwave absorption frequencies and increase absorption intensities. Adv. Mater. *26*, 8120–8125. https://doi.org/10.1002/adma.201403735.

52. Li, Y., Li, X., Zhu, M., Xing, Z., Chen, T., and Zhao, J. (2025). Analysis of resonant characteristics of microwave actuators at different frequencies. Sensor Actuator Phys. *387*, 116444. https://doi.org/10.1016/j.sna.2025.116444.

53. Ai, Y., Xing, R., Ren, N., Huang, R., Cui, M., Su, R., and Kong, J. (2025). Biomass-derived hierarchical carbon frameworks enable robust microwave absorption. Matter *8*, 102289. https://doi.org/10.1016/j.matt.2025.102289.